JOURNAL OF THERMOPHYSICS AND HEAT TRANSFER
Vol. 9, No. 3, July–September 1995

Characterization of a Nitrogen Flow Within a Plasma Wind Tunnel

Stefanos Fasoulas,* P. Christian Sleziona,* Monika Auweter-Kurtz,† Harald A. Habiger,‡ Stefan H. Laure,* and Anja T. Schönemann‡
University of Stuttgart, Stuttgart D-70550, Germany

This article presents a comparison of numerical and measured results of a nitrogen high-enthalpy flow. Experimental data at a first cross section are used as initial and boundary conditions for a numerical simulation of the high-enthalpy flow, the results at a second cross section are compared with the numerical solution. The program system employed to examine the flow consists of a Navier–Stokes flowfield solver including models to investigate thermal and chemical nonequilibrium flows. Different measurement techniques were applied to determine the flowfield properties. The measurements made possible the calculation of the local specific enthalpy and mass flux distributions of the plasma plume by basic thermodynamic equations. These mass flux distributions are compared with measurements by mass spectrometry. Special emphasis is also placed on the investigation of the catalytic activity of different materials.

Nomenclature

c = molar concentration
$c_{p_{\mathrm{rot+trans}}}$ = portion of the translational and rotational DOF to heat capacity at constant pressure
D = diffusion coefficient
E = energy
H = enthalpy
h = specific enthalpy
h_{N}, h_{N^+} = dissociation, ionization enthalpy
I = current
$\bar{\bar{I}}$ = unit matrix
K = constant, defined in Eq. (1)
k = Boltzmann constant
k_f,k_b = forward/backward reaction rate
k_w = catalytic rate recombination constant
Le = Lewis number
M = molecular mass
$\dot{m}$ = mass flow rate
n = number density
p = pressure
$\dot{q}$ = heat flux
R_{cyl} = radius of cylinder
R_{eff} = effective radius of body
$\mathcal{R}$ = gas constant
Sc = Schmidt number
T = temperature
u = internal energy
v, v = velocity
x = axial distance to plasma source
y = radial distance to center of jet
α = coupling coefficient
β = velocity gradient
γ_R = recombination efficiency
λ = thermal conductivity
μ = absolute viscosity
ν = stoichiometric number
ξ = mass fraction
ρ = density
τ = relaxation time
$\bar{\bar{\tau}}$ = stress tensor
φ = number for catalytic activity defined in Eq. (6)
ψ = mole fraction
ω = chemical source term

Subscripts
A = atomic
e = boundary-layer edge
e = electron
fc = fully catalytic
rot = rotational
s = stagnation point
tot = total
trans = translational
vib = vibrational
w = wall
∞ = freestream

Presented as Paper 93-2817 at the AIAA 28th Thermophysics Conference, Orlando, FL, July 6–9, 1993; received March 15, 1994; revision received Sept. 15, 1994; accepted for publication Oct. 31, 1994.

*Research Engineer, Institut für Raumfahrtsysteme, Electric Propulsion and Plasma Technology Division.
†Professor, Institut für Raumfahrtsysteme, and Head, Electric Propulsion and Plasma Technology Division. Member AIAA.
‡Research Scientist, Institut für Raumfahrtsysteme, Electric Propulsion and Plasma Technology Division. Member AIAA.

I. Introduction

LABORATORY plasmas and high-enthalpy flows are produced for many various applications and technologies, e.g., spraying, coating, welding, and waste treatment. A space-related application is the simulation of the entry conditions of a spacecraft entering into the Earth's atmosphere or into atmospheres of other celestial bodies. This topic is divided in two basic research areas. In so-called hot shot tunnels[1] or in piston shock tunnels[2] special emphasis is placed on the investigation of the aerodynamic properties by reproducing the characteristic Mach–Reynolds numbers relation during the atmospheric entry. However, the test runs at these experimental plants are limited to a few milliseconds, which is far too short for the study of the erosion behavior of spacecraft thermal protection materials and systems (TPS).

This research area is usually performed in arc-heated wind tunnels. Within the wind tunnels the flow is generally produced by two different kinds of plasma sources: 1) the thermal plasma generators (TPG) or 2) magnetoplasmadynamic generators (MPG). These two types differ mainly in their acceleration concept.[3] In wind tunnels equipped with TPG,[4–9] the test gas is heated by an electric arc and usually accelerated

through a nozzle. The two plasma wind tunnels PWK1 and PWK2 at the Institut für Raumfahrtsysteme (IRS) of the University of Stuttgart are equipped with MPG devices,[10] in which magnetoplasmadynamic forces further accelerate the gas. All plasma wind tunnels are connected to pumping systems at the IRS to a roots pump system with a total suction power of more than 300,000 m^3/h. This pumping system is regulated so that the background pressure in the test chamber can be chosen independently from the mass flow rate.

How well the tests in the wind tunnels reproduce or simulate the real entry conditions can only be determined by comparing the numerical predictions or the measurement data (if available) of the flight environment with the flow parameters in the wind tunnels. Both the use of theoretical models as well as the application of the different measurement methods for the determination of the flow properties are handicapped and more complicated by the character of the flow that is usually in thermal and chemical nonequilibrium. A complete characterization of such flows would require the measurement of the number density, velocity, translational, rotational, vibrational, and excitation temperatures of each present heavy particle species and the electron temperature and density, respectively, at every spatial position of the flow. Of course, measurements in this detail are not possible yet. A summary of the currently available intrusive and nonintrusive diagnostic techniques for high enthalpy flows is given in Ref. 11. To determine or to estimate the experimentally not accessible parameters, the measurements have to be accompanied by numerical or theoretical means. This allows also the calibration of the theoretical models by the available measurement data. Moreover, since these models are similar or even identical to those used for the prediction of real re-entry flows, it is possible to obtain an experimentally qualified numerical code for the calculation of flows in thermal and chemical nonequilibrium.

Thus, to qualify different measurement techniques, to demonstrate the reliability of the re-entry simulation in the PWK environment, and to test and calibrate theoretical methods, an extensive experimental survey was performed at the IRS. The description of the experimental methods may be found in Refs. 10, 13, and 14, and most of the obtained results for this program are published in Ref. 12.

This article mainly addresses the comparison of a Navier–Stokes calculation including thermal and chemical nonequilibrium with the measurements and a brief summary of the proceeding to obtain the local specific enthalpy and mass flux distributions. Only some selected and additional experimental results will be presented here, e.g., mass spectrometry and a first investigation about the catalytic activity of different materials.

For numerical investigation the high-enthalpy flow solver HEFLOS is used as a three-dimensional axisymmetric program system. HEFLOS was developed for calculations of magnetoplasmadynamic thrusters,[15] with ionized argon as an ideal gas flowfield. A nonequilibrium air chemistry is introduced for the plasma wind-tunnel applications.[16] This program system is based on the finite volume code NSFLEX[17,18] using MUSCL-type flux difference splitting. For the pure nitrogen flow calculations the Navier–Stokes flowfield solver is extended by the nitrogen species conservation equations, a vibrational and an electron energy equation. The chemical source term of the species conservation equations is calculated by the Park model.[19–21] In accordance with this model a step towards thermal nonequilibrium is taken by distinguishing between the heavy particle translational temperature, assumed to be equal to the rotational temperature, and the electron and vibrational temperatures, which are calculated separately by two additional energy equations. Thus, the flowfield in the plasma wind tunnel is calculated in thermal and chemical nonequilibrium where a suitable three-temperature model for the source terms is utilized.

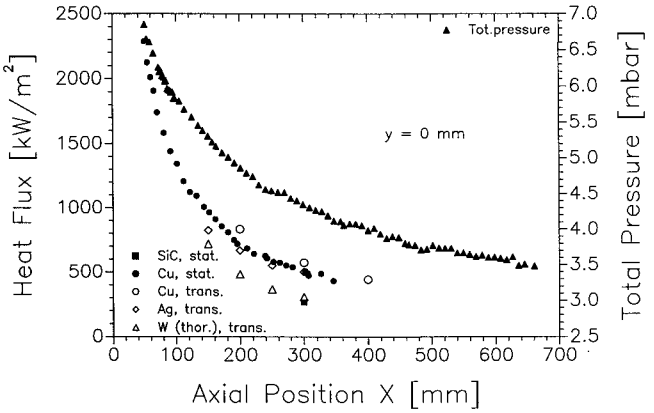

Fig. 1 Total pressure and heat flux vs axial position (stat.: stationary, trans.: transient.

II. Test Conditions and Measurements

As a first step a pure nitrogen plasma flow was chosen in order to keep the complexity of the flow easier to grasp and to simulate the conditions that result in a maximum calculated temperature at the leading edge for a re-entry vehicle like HERMES.[22] The parameters for the flight environment are, altitude 81.3 km, a velocity of 7452 m/s that corresponds to a specific freestream enthalpy of 28 MJ/kg, a specific mass flow rate of 0.117 $kg/(m^2s)$, and a total pressure of 4 mbar.

Because these conditions are not directly adjustable within the plasma wind tunnel, an interpolation procedure was necessary to obtain the values for the current, mass flux, ambient pressure, and the distance to the plasma source. The directly adjustable parameters that were obtained after this procedure are, total mass flux of 1.33 g/s or 63.8 sl/min nitrogen, current of 750 A, and ambient pressure of 2.9 mbar. At these conditions the necessary total electrical power input is about 38 kW with an efficiency of the plasma source of about 68%, resulting in a mean specific enthalpy of 19.3 MJ/kg at the exit of the nozzle. The required simulation conditions were approximately met at a distance of $x = 300$ mm. This position $x = 300$ mm was then chosen as the second cross section of the program. A first cross section that should be used as initial or boundary condition was fixed at a position of $x = 50$ mm.

Different experimental methods, e.g., pitot pressure, heat flux and electrostatic probes, mass spectrometry and Fabry–Perot interferometry, were then applied to determine the flowfield properties at the two specified cross sections and their axial development. As an example the total pressure depending on the axial distance to the plasma source and the results of the heat flux measurements with different catalytic materials as probe inserts are shown in Fig. 1. The dependence of the heat flux upon the catalytic activity of the material will be discussed in more detail in Sec. IV.

III. Calculations of the Local Specific Enthalpies and Mass Fluxes

The mean enthalpy at the plasma source exit of 19.3 MJ/kg results from a local distribution of the specific enthalpy. Additionally, the average value at a certain cross section as well as the distribution of the specific enthalpy depend on the axial position. A method to investigate the local specific enthalpy in the freestream plasma flow is given by the theory of heat transfer. Two methods will be described briefly as follows:

A. First Method

Pope, Vojvodich, and Marvin[24–26] approximated a relationship between the fully catalytic heating rate and the enthalpy for a frozen freestream flow as

$$\dot{q}_{fc} = K(p_{tot}/R_{eff})^{0.5} h_{tot,e} \tag{1}$$

$h_{tot,e}$ may be assumed to be equal to the freestream enthalpy $h_{tot,\infty}$, and R_{eff} is an effective probe nose radius given by[23,27] $R_{eff} = 2.9R_{cyl}$ for a cylindrical probe with radius R_{cyl}. Although the copper surface of the heat flux probes has a high recombination efficiency, it may not be considered fully catalytic with respect to the recombination of the atoms. Goulard[28] and Pope[23] derived a theory that allows the estimation of the ratio of the heating rate at a partially catalytic surface to the equivalent heating rate at a fully catalytic surface. This ratio depends on the local freestream enthalpy. This method was used here to calculate the equivalent fully catalytic heat flux from the measured heat flux on the copper probe.

With the known pressure distribution (Fig. 1) it is possible to calculate the local specific enthalpy with Eq. (1). Additionally, it is possible to determine a mean specific enthalpy by integrating the local enthalpy distribution. The average enthalpy at the first cross section is calculated to be 21.5 MJ/kg, which compares quite well with the mean enthalpy determined at the plasma source exit by measurement (19.3 MJ/kg). On the other hand, the mean value at the second cross section ($x = 300$ mm) of 7.6 MJ/kg indicates losses of specific energy of the plasma flow, which is mainly caused by the entrainment of ambient gas. The radiation losses are estimated to be less than 5%. The engulfment of ambient gas will increase the total mass flow of the jet and therefore decrease the specific energy. The ratio of the energy losses by this effect will be about 2.4. Therefore, the total mass flux rate at the position $x = 300$ mm should be about 3.2 g/s. The maximum specific enthalpy calculated with Eq. (1) is 85.9 MJ/kg at $x = 50$ mm and 26.6 MJ/kg at $x = 300$ mm, respectively, at the center of the jet.

B. Second Method

The relationship used in the theory derived by Fay and Riddell[29] to determine the local specific enthalpy is more detailed. They suggested a correlation equation that represented best their numerical integration of the heat flux on a fully catalytic wall (see also Ref. 30):

$$\dot{q}_{fc} = 0.937(\rho_s\mu_s/\rho_\infty\mu_\infty)^{0.1}(\beta\rho_\infty\mu_\infty)^{0.5}(h_{tot,\infty} - h_s) \qquad (2)$$

Because of the chemical and thermodynamic nonequilibrium of the flow, the values for the average molecular mass for the gas mixture and the ratio of the specific heats are not known exactly. They can only be calculated if the local specific enthalpy is already determined. Thus, the necessary data for ρ_∞ and ρ_s are not known. Therefore, Eq. (1) was used to obtain a first approximation of the local specific enthalpy distribution. With the obtained values for the specific enthalpy the species mass fractions were then calculated. Finally, the extended theory of heat transfer [Eq. (2)] was used to check the enthalpy values determined before. A comparison of the results of both methods is shown in Fig. 2 for an axial profile.

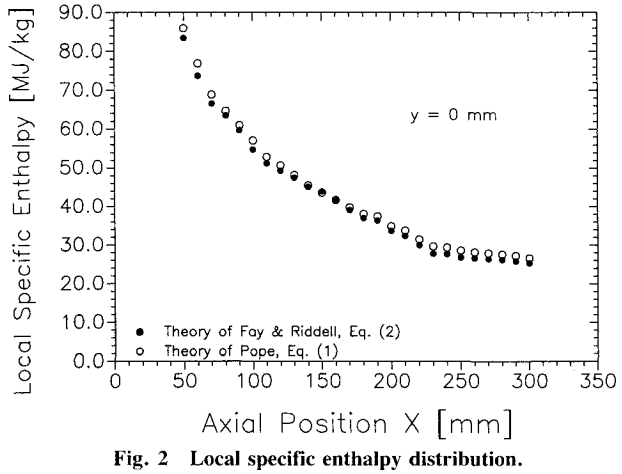

Fig. 2 Local specific enthalpy distribution.

The values obtained with Eq. (2) correspond very well to those calculated with Eq. (1). The maximum enthalpies determined with this method are 83.4 MJ/kg at $x = 50$ mm and 25.3 MJ/kg at $x = 300$ mm, respectively, at the center of the jet. The distributions obtained with Eq. (2) can also be integrated yielding average specific enthalpies of 20.2 MJ/kg at $x = 50$ mm and 7.1 MJ/kg at $x = 300$ mm. Again, both values are similar to those calculated with Eq. (1), and the value at the first cross section agrees very well with the measured quantity of 19.3 MJ/kg at the plasma source exit.

C. Local Mass Flux

Knowing the local enthalpy, the species concentrations of the nitrogen plasma (assumed to consist of the species N_2, N, N^+ and e^-) can be calculated with the energy equation, if the heavy particle temperature, velocity, ambient pressure, and electron density and temperature are measured or known.[12] The main assumptions for this calculation are 1) the ambient pressure is equal to the static pressure, 2) quasineutrality—density of the ions is equal to the electron density, 3) only single ionized atomic nitrogen is considered, and 4) mixture of ideal gases with two temperatures ($T_{rot} = T_{trans} = T_\infty$, $T_{vib} = T_e$).

The energy conservation equation may then be written as

$$h_{tot,\infty} = \tfrac{1}{2}v_\infty^2 + c_{p_{rot+trans}}T_\infty + \xi_{N_2}h_{vib} + \xi_N h_N + \xi_{N^+}h_{N^+} \qquad (3)$$

With the calculated values for the local specific enthalpy, the measured ambient pressure and the measured distributions for the velocity, electron density and temperature, and heavy particle temperature, it is now possible to calculate the local species mass and mole fractions of the pure nitrogen plasma flow. Detailed results for the species number densities will be presented in comparison with numerical values in Sec. VI. The multiplication of the species number densities with their velocity and mass yields local specific mass fluxes of the species.

At the position $x = 50$ mm, the mole fraction of dissociated nitrogen is calculated to be about 60% and the fraction of the ions is nearly 20%. With increasing distance the ionized fraction becomes smaller, reaching a value of only 0.17%, while the dissociation mole fraction is about 68% at $x = 300$ mm. This is a very important result for the assessment of material tests, which are performed typically at such positions or even further downstream.

Another very interesting value is the total specific mass flux at the center of the jet at the position $x = 300$ mm. This value is determined to be about 0.128 kg/(m²s), which is only 9.4% higher than the required value of 0.117 kg/(m²s). Thus, all required simulation parameters (local specific enthalpy, total pressure, and local specific mass flux) were reproduced simultaneously within the PWK-IRS.

A verification of the obtained mole fractions is possible by integrating the total specific mass flux over the plasma jet diameter. This integration yields for the inflow cross section a mass flow rate of 1.29 g/s, which compares very well to the mass flux fed through the plasma source (1.33 g/s). The calculated mass flux at the outflow cross section is about 3.14 g/s, which is 2.36 times the input mass flux and which corresponds very well to the loss of the average specific enthalpy of the plasma flow due to the suction of ambient gas (about 2.4).

The mole fractions were also determined experimentally by mass spectrometry. Because of the sensitivity of the mass spectrometer concerning high thermal loads, the measurements were carried out only at $x = 300$ mm. A correction factor concerning the recombinations of atoms due to the orifice dimensions is applied to the data. Results are shown in Fig. 3 in addition to the mole fractions calculated with Eq. (3). The comparison shows a very good agreement. The assumption that only N^+-ions (and no N_2^+-ions) are present in

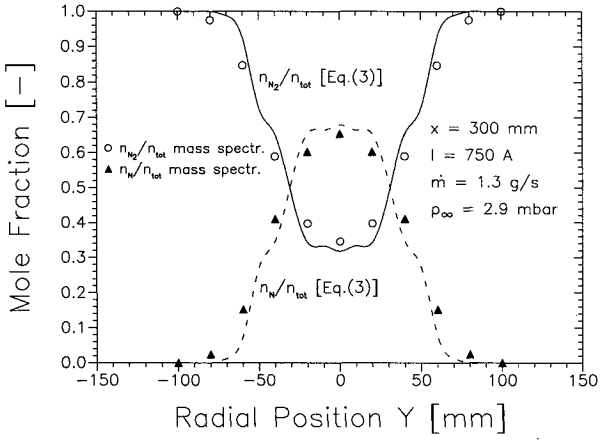

Fig. 3 Comparison of the calculated and the measured mole fractions vs radial position.

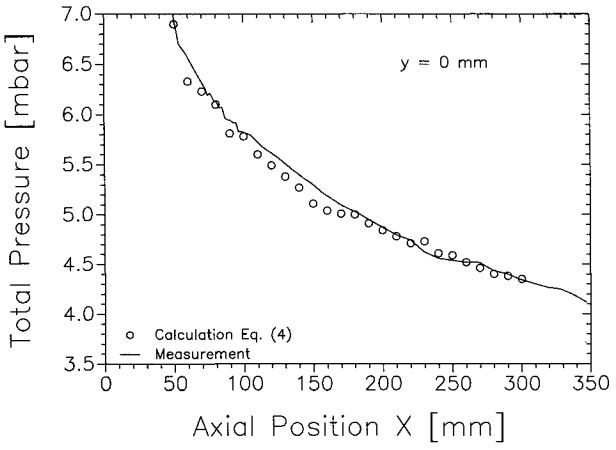

Fig. 4 Comparison of the calculated and the measured total pressure vs axial position.

the jet is verified with the mass spectrometer. The analysis of the residual gas inside the wind tunnel showed also a small amount of 1.1% O_2 in the center of the jet, and about 2.4% outside of the jet.

Additional verification of these results is possible by applying the Bernoulli equation for compressible flows to calculate the total pressure and comparing it to the measured. Basically, Bernoulli's equation for compressible flows reads:

$$(p_s/\rho_s) + u_s + \tfrac{1}{2}v_s^2 = (p_\infty/\rho_\infty) + u_\infty + \tfrac{1}{2}v_\infty^2 \qquad (4)$$

A comparison of the calculated to the measured pressure as axial profile is shown in Fig. 4. The agreement with the measured data is good (within 10%). Deviations may occur because of the high sensitivity of the presented method to small inaccuracies in the determination of the freestream velocity. On the other hand, because of the small portion of the kinetic energy to the total energy of the flow, the velocity has only minor influence for the determination of the mole fractions with the energy conservation equation [Eq. (3)].

IV. Effects of Different Surface Catalytic Activity

The method described briefly in Sec. III, also known as heat flux method,[11,23] has the uncertainty that the catalytic recombination efficiency of the surface of the heat flux probe must be known for the calculation of an equivalent fully catalytic heat flux. In addition, the effective radius R_{eff} must be determined analytically or by experiment. Although the factor $R_{eff}/R_{cyl} = 2.9$ (Refs. 27 and 28) used within this program resulted in a good approximation of the specific enthalpy, it is not certain whether it is applicable generally. In Ref. 25 this factor was found to be about 2.3, in Ref. 11 it is given as 1.85, the results of Ref. 28, however, give higher values ranging from 2.9 to 3.7.

In the present case of a pure nitrogen plasma and with the performed measurements these uncertainties can be avoided by solving simultaneously the Bernoulli equation [Eq. (4)], the energy equation [Eq. (3)], and the heat transfer relation according to Fay and Riddell [Eq. (2)] or any other heat transfer theory. This method will be introduced here for the discussion of the effects of different surface catalytic activity on the heat flux transferred to a body exposed to the plasma flow. The procedure is as follows (see also Fig. 5): for a given specific enthalpy (x axis in Fig. 5), and with the measured electron density, the neutral species concentrations of the flow are calculated with Eq. (3). Then, with the obtained results, the measured heat flux, and a varying ratio of $\dot{q}/\dot{q}_{fc}$ the specific enthalpy according to the heat transfer theory, i.e., Eq. (2), is determined. The quotient of this calculated to the given specific enthalpy is depicted as y axis in Fig. 5. Finally, the total pressure is calculated with Eq. (4) and the ratio to the measured pressure is also depicted as y axis in Fig. 5. The solution for the specific enthalpy as well as the quotient $\dot{q}/\dot{q}_{fc}$ is then given as the point of intersection of the total pressure curve with the straight line $h_{calc}/h = 1$.

Figure 5 shows the result for the stationary copper probe at a distance of $x = 50$ mm to the plasma source. The ratio $\dot{q}/\dot{q}_{fc}$ is found to be 0.782, corresponding well with the estimated value used for the calculation in Eq. (1). The specific enthalpy is 81.5 MJ/kg [for comparison $h = 85.9$ MJ/kg with Eq. (1)]. Figure 6 depicts the result for a thoriated tungsten probe at a distance of $x = 300$ mm. Here, the solution is

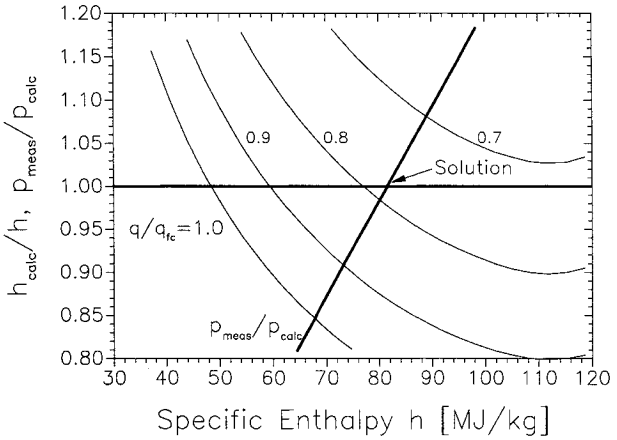

Fig. 5 Determination of the specific enthalpy and the ratio $\dot{q}/\dot{q}_{fc}$ for the stationary copper probe at the position $x = 50$ mm, $y = 0$ mm.

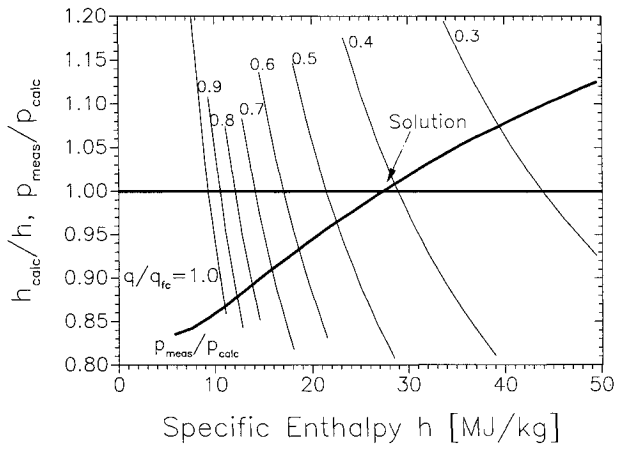

Fig. 6 Determination of the specific enthalpy and the ratio $\dot{q}/\dot{q}_{fc}$ for the transient tungsten probe at the position $x = 300$ mm, $y = 0$ mm.

Table 1 Comparison of the measured and the theoretical heat flux ratios

Surface material	γ_R	T_w, K	k_w,[a] m/s	k_w,[b] m/s	Axial position, mm	h_∞, MJ/kg	$(\dot{q}/\dot{q}_{fc})_{calc.}$ Eqs. (5) and (6)	$(\dot{q}/\dot{q}_{fc})_{meas.}$
Cu, stationary cooled	0.059	320	10.3, Ref. 23	10.2	300	27.4	0.71	0.70
	—	—	—	9.5	250	29.6	0.71	0.69
	—	—	—	10.7	200	34.8	0.72	0.73
	—	—	—	12.0	150	40.8	0.75	0.79
	—	—	—	9.5	100	56.5	0.73	0.73
	—	—	—	8.5	50	81.5	0.82	0.78
Cu, transient	0.10	500	22.0, Ref. 33	23.0	300	27.4	0.76	0.77
	—	—	—	24.0	200	34.8	0.78	0.80
W, (thoriated) transient	0.0087	400	—	1.7	300	27.4	—	0.42
	0.010	430	—	2.1	250	29.6	—	0.44
	0.014	500	—	3.0	200	34.8	—	0.47
	0.016	530	—	3.6	150	40.8	—	0.59
Ag, transient	0.046	500	10.0, Ref. 23	10.2	300	27.4	0.66	0.68
	—	500	—	10.2	250	29.6	0.64	0.65
	—	500	—	10.3	200	34.8	0.65	0.66
	0.045	600	—	10.6	150	40.8	—	0.68
SiC, transient	0.0041	500	—	0.9	300	27.4	—	0.37
SiC, stationary	0.0054	1438	—	2	300	27.4	—	0.36

[a]From literature. [b]From pressure measurements.

found at an enthalpy of 27.4 MJ/kg [Eq. (1): $h = 26.6$ MJ/kg]. This figure clarifies also the limits of the presented method. With the estimated error of about 5% for the total pressure measurements,[12] this would result in a possible error of the specific enthalpy of about 30%. Therefore, an accurate pressure measurement is required for the confident calculation of the parameters. The presented method also fails if the dependence of the dynamic pressure on the specific enthalpy is low, e.g., at low enthalpies outside of the center of the plasma flow.

The ratio of the heating rate at a partially catalytic surface to the heating rate at a fully catalytic surface can also be evaluated theoretically.[28] If it is assumed that all investigated metallic surfaces are fully catalytic for ions and that the ionic recombination produces only atoms, $\dot{q}/\dot{q}_{fc}$ may be written as

$$\frac{\dot{q}}{\dot{q}_{fc}} = 1 - \frac{Le^{2/3}(\xi_N + \xi_{N^+})(h_N/h_\infty)}{1 + (Le^{2/3} - 1)(\xi_N + \xi_{N^+})(h_N/h_\infty)}(1 - \varphi) \quad (5)$$

where φ is given by the equation

$$\varphi = \{1/[1 + (0.47\sqrt{2\beta\mu_{se}\rho_{se}}/Sc^{2/3}\rho_w k_w)]\} \quad (6)$$

The Lewis number is assumed for simplification as $Le = 1$ for both, neutral particles and ions, in the following, and μ_{se} and ρ_{se}, the viscosity and the density at the stagnation point outside of the boundary-layer edge, are assumed to be equal to the freestream values for the present subsonic flow case. The catalytic rate recombination constant may be calculated from the wall recombination efficiency γ_R as[28]

$$k_w = \gamma_R(\Re T_w/2\pi M_A)^{1/2} \quad (7)$$

However, the wall recombination efficiency defined as a ratio of atoms recombining on a surface to the total number of atoms striking the surface is not a constant, but may vary, e.g., with the wall temperature. Table 1 lists some results obtained with the different catalytic probes and compares the determined heat flux ratios with the theoretical ones according to Eq. (5). Results are only presented for the test points where at least four measurements were performed. The reproducibility of these measurements was within 5%. If a value for k_w was available from the literature it is marked with the corresponding reference number. For comparison, this value is also calculated from the present measurements. The copper and tungsten probes show a higher dependence of the catalytic recombination efficiency on the surface temperature than silver. A value for the catalytic rate of pure tungsten is given in Ref. 25 with $k_w = 0.3$ m/s at 350 K. However, the thoriated tungsten (W + 2% ThO_2) used here was expected to have a slightly higher recombination efficiency, as shown also with the performed measurements. The catalytic rate for silver from Ref. 25 is given for a surface temperature of 350 K. With this value the heat flux ratio at a surface temperature of 500 K was only slightly underestimated. The increase of the surface temperature for the silver probe has therefore only minor effects on the catalytic recombination efficiency, as it is also shown by the measurements at 600 K. The tests with the SiC probe in the stationary mode were performed with the typical material support system used at the IRS for tests of fiber-reinforced ceramic materials. The surface temperature was measured with a high accuracy pyrometer and the resulting radiation heat flux is increased by 30% to include heat flux losses to the support system. It should be mentioned that the erosion of the SiC probe during this test of 20 min was negligible.

The measured values compare generally well with the theoretical ones. Therefore, if the catalytic recombination efficiency of the different materials is known exactly, the described method could also be used for the determination of other flowfield properties, e.g., gas temperature[31] or velocity. For materials with unknown recombination efficiency, however, this method can be used to determine it. In the case of an air plasma flow, materials with different catalytic behavior with respect to the recombination of nitrogen and oxygen atoms could be used for the determination of the atomic oxygen and nitrogen mass flux (e.g., AgO).[23,32]

Finally, Fig. 7 shows the variation of the heat transfer rate parameter with the total enthalpy for the nitrogen plasma flow and a comparison with values from the literature.[23,33,35] This figure clarifies again the influence of the surface temperature, surface material, and effective probe radius. The measurements of Ref. 33 were performed at a surface temperature of 1000 K, resulting in a higher heat transfer rate. The results from Ref. 23 indicate that the heat transfer rate is increasing with decreasing effective radius. However, the results obtained at the IRS do not fit exactly in this prediction concerning the value of the effective radius. The difference could be explained by different surface temperatures (IRS: cold wall, stationary, Ref. 23 transient measurements) and by the different test facilities. In the MPG facility of the IRS the portion of the dissociation enthalpy to the total enthalpy in the freestream may be higher than in the arc-heated facility

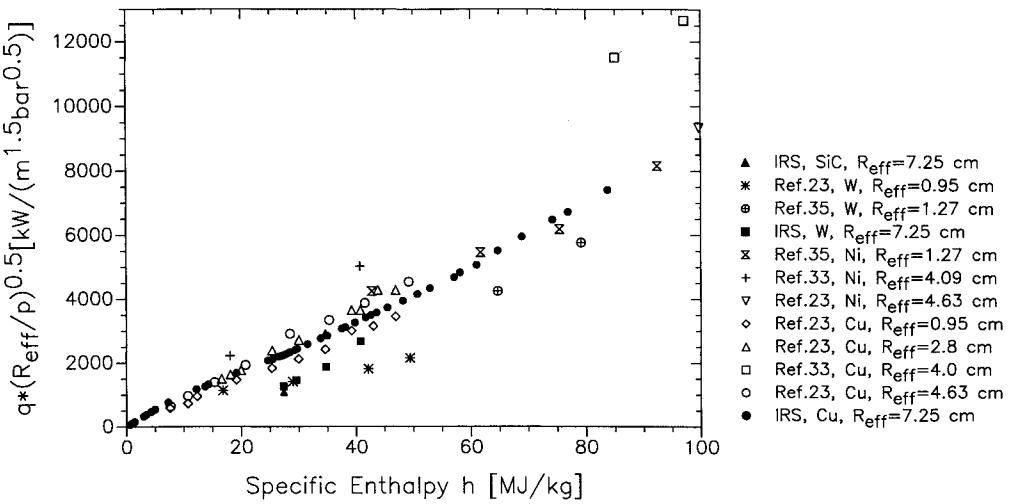

Fig. 7 Heat flux rate parameter vs specific enthalpy.

used in Ref. 23. Nevertheless, taking into account that the catalytic rate constants are given with an error bar of 30–50%, the agreement is quite good.

V. Numerical Model

The nonequilibrium nitrogen flow that was heated by an electrical discharge is calculated starting with the measurement data of the inflow cross section (x = 50 mm). For the calculation it is furthermore assumed that the flow is axisymmetric, that the static pressure is constant throughout the whole computational domain, and that no arc current is present anymore beyond this first cross section.

The numerical model presented in this section was developed for calculations of an axisymmetric high-enthalpy flow. The governing equations are used to describe the viscous nitrogen flow in thermal and chemical nonequilibrium. Three different temperatures are considered in the nitrogen flow: 1) heavy particle, 2) electron, and 3) vibrational temperature. The extension of the method to include air as fluid medium is straightforward and has already been done. Since the ionization is not negligible for the problem presented in this article, it is necessary to solve also the electron energy equation. Due to the exchange of vibrational energy, this conservation equation has also to be included. The complete set of equations that is necessary to describe generally nonequilibrium plasma flows is the following:

Total mass conservation:

$$\frac{\partial}{\partial t}\rho + \nabla\rho v = 0 \tag{8}$$

Momentum conservation:

$$\frac{\partial}{\partial t}\rho v + \nabla\rho v \otimes v = \nabla(-p\bar{\bar{I}} + \bar{\bar{\tau}}) \tag{9}$$

Total energy conservation:

$$\frac{\partial}{\partial t}E + \nabla(H)v = \nabla(\bar{\bar{\tau}}v) + \nabla\lambda\nabla T + \nabla\lambda_{\text{vib}}\nabla T_{\text{vib}} + \nabla\lambda_e\nabla T_e + \nabla\sum_{i=1}^{5} H_i D_i \nabla\psi_i \tag{10}$$

Species conservation (in molar concentrations c_i):

$$\frac{\partial}{\partial t}c_i + \nabla c_i v = \omega_i + \nabla\frac{\rho}{M_i}\nabla\psi_i \tag{11}$$

Vibrational energy conservation:

$$\frac{\partial}{\partial t}E_{\text{vib}} + \nabla E_{\text{vib}} v = \nabla\lambda_{\text{vib}}\nabla T_{\text{vib}} + \nabla E_{\text{vib}} D_{N_2}\nabla\psi_{N_2} + \omega_{N_2} D_{N_2} + \frac{E_{\text{vib}}(T) - E_{\text{vib}}(T_{\text{vib}})}{\tau_{N_2}} + \frac{M_{N_2}}{M_e}\frac{E_{\text{vib}}(T_e) - E_{\text{vib}}(T_{\text{vib}})}{\tau_{e-N_2}} \tag{12}$$

The last two terms on the right side of this equation represent Landau–Teller type coupling of the vibrational temperature to the heavy particle and electron temperature, respectively.

Electron energy conservation:

$$\nabla\left(\frac{3}{2}n_e k T_e v\right) + \nabla q_e^* = -p_e\nabla v + \sum_{i=1}^{4} n_i n_e \alpha_{ei}(T - T_e) - \sum_{r=\text{ion}} \omega_{e,r} h_{re} + \nabla\frac{5}{2}n_e k T_e D_e \nabla\psi_e - \frac{M_{N_2}}{M_e}\frac{E_{\text{vib}}(T_e) - E_{\text{vib}}(T_{\text{vib}})}{\tau_{e-N_2}} \tag{13}$$

The second term on the right side denotes the coupling of the electron temperature to the heavy particle temperature, the third term represents the reaction losses due to ionization processes.

The Yos model[34] was used for the transport coefficients. Mass diffusion is implemented in the appropriate equations, while thermal and pressure diffusion are neglected. Radiation losses are not considered since these losses are very small compared to other energy transport mechanisms. Due to the special importance for the modeling of the chemical and thermal nonequilibrium, the chemical kinetic model to determine the chemical source term will be described in more detail in the following:

A. Chemical Model

The modeling of the chemical kinetics is based on the air model of Park.[19–21] Again, since the results presented here are for nitrogen, only the reduced chemical reaction system of these species is presented. However, the complete air system is now implemented at the IRS and is presently validated. For nitrogen, the following reactions have been considered:

Dissociation reactions:

$$N_2 + N \Leftrightarrow N + N + N \tag{14}$$

$$N_2 + N_2 \Leftrightarrow N + N + N_2 \quad (15)$$

$$N_2 + N^+ \Leftrightarrow N + N + N^+ \quad (16)$$

$$N_2 + N_2^+ \Leftrightarrow N + N + N_2^+ \quad (17)$$

$$N_2 + e \Leftrightarrow N + N + e \quad (18)$$

Charge exchange reaction:

$$N_2 + N^+ \Leftrightarrow N + N_2^+ \quad (19)$$

Associative ionization:

$$N + N \Leftrightarrow N_2^+ + e \quad (20)$$

Electron impact ionization:

$$N + e \Leftrightarrow N^+ + 2e \quad (21)$$

The chemical production rate of a species i is modeled as

$$\omega_i = \sum_{j=1}^{m} (\nu''_{ij} - \nu'_{ij}) \left(k_{fj} \prod_i c_i^{\nu'_{ij}} - k_{bj} \prod_i c_i^{\nu''_{ij}} \right) \quad (22)$$

The sum extends over all participating reactions m. This equation represents a coupled and stiff system of differential equations. An adequate time step procedure has been developed for this production term.

The forward k_{fj} and backward reaction rates k_{bj} are implemented in accordance with the thermal nonequilibrium model. Park's model as given in Ref. 20 was chosen and improvements outlined in Ref. 21 are implemented. The equilibrium constants are taken from Ref. 19. The reaction coefficients are given in the usual form, i.e., for the forward coefficient

$$k_f = CT_{x,f}^n e^{-T_d/T_{x,f}} \quad (23)$$

where $T_{x,f}$ is the controlling temperature of the reaction under consideration; it can be T, T_v, T_e, or $T_a = \sqrt{TT_f}$.

The rate constant for the backward reactions is determined using the equilibrium constant K:

$$k_b = \frac{k_f(T_{x,b})}{K(T_{x,b})} \quad (24)$$

The temperature $T_{x,b}$ is the controlling temperature of the backward reaction. Park gives the equilibrium constants K as a polynomial of third order of the logarithm of temperature:

$$K(T_{x,b}) = \exp(A_1 + A_2 \ln Z + A_3 Z + A_4 Z^2 + A_5 Z^3) \quad (25)$$

where the variable Z is defined as $Z = 10{,}000/T_{x,b}$. The values of the used coefficients A_1–A_5 may be found in Refs. 19–21.

B. Solution of the Equation Systems

The equation system Eqs. (8–13) is divided in three parts and solved in the following sequence: 1) flowfield code [Eqs. (8–10)], 2) chemical and vibrational energy code [Eqs. (11) and (12)], and 3) electron energy code [Eq. (13)].

For the calculation of the high-enthalpy flow, the electron energy, the vibrational energy, the nonequilibrium chemical reactions, and the flowfield codes are correlated to determine flowfield, electron temperature, vibrational temperature, and the species density distributions of nitrogen. These three codes are connected in the following manner: For a given flowfield, the electron temperature and, hence, the chemical composition including the vibrational energy equation is determined. With these results, in the next iteration step, the flowfield equations are integrated. This new flowfield and the new distribution of the electron temperature are taken to calculate the new chemical properties and the new vibrational temperature distribution, etc. These sequences are repeated until the calculated values, such as flowfield, chemical, vibrational temperature, and electron temperature distribution reach numerical equilibrium. The flowfield was calculated until the residuals were decreased more than five orders of magnitude. For the other components of the computational system the same criterion was chosen as a determination of a converged solution.

The nonlinear, elliptical, partial differential equation [Eq. (13)] is solved with a finite difference method. The discretization yields a nonlinear equation that is iteratively solved with a modified Gauss–Seidel algorithm. The nonlinear, hyperbolic, partial differential equations for the flowfield [Eqs. (8–10)] are solved with a finite volume method. Here, the NSFLEX code[17,18] is used, modified for an inhomogeneous state. The equations that represent the chemical reactions [Eq. (11)] and the vibrational energy equation [Eq. (12)] are solved with an explicit MacCormack predictor–corrector algorithm.

All equations used for the iteratively solved high-enthalpy flow are coupled completely by corresponding source terms which correlate the different physical processes and their corresponding conservation equations to one another. The fact that the conservation equations are solved by three individual solution procedures does not reduce the coupling intensity among the different equations, it represents only a solution and program developing strategy. These individual solution procedures enable an easier and faster implementation of different physical processes. With an individual procedure the calculation and the boundary conditions can be adjusted exactly for various problems. Finally, different types of differ-

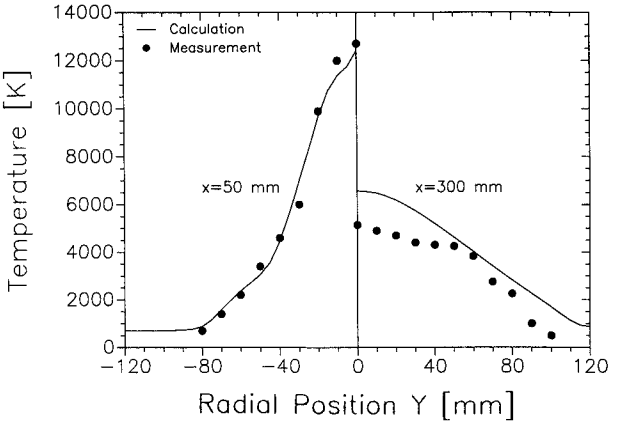

Fig. 8 Heavy particle temperature at the two cross sections.

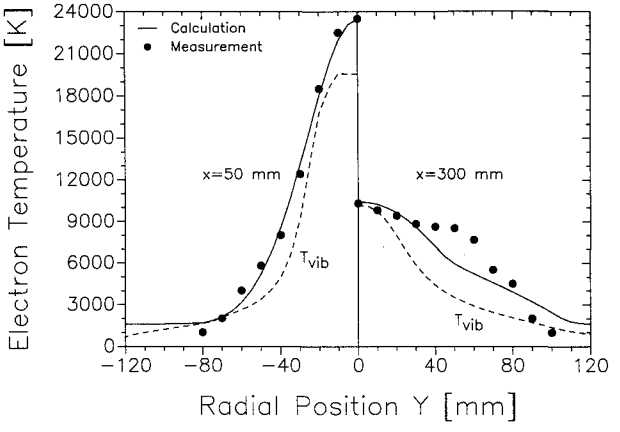

Fig. 9 Electron temperature at the two cross sections.

ential equations require different suitable solution procedures.

VI. Comparison Measurement-Calculation

For the numerical simulation of the nitrogen plasma flow a data set based on the experimental results at the inflow cross section (x = 50 mm) is used as the starting parameter, except the vibrational temperature and the number density of ionized molecules N_2^+, which are extrapolated backwards from the flow. The flow is considered to be axisymmetric. Two grids were used for the calculation consisting of 33 × 27 and 63 × 51 grid points, respectively, in the axial x and radial y direction. The influence of the grid refinement on the obtained results and the convergence of the solution was negligible. The flowfield [Eqs. (8–10)] was calculated with a finite volume solver in the center of the grid cells, whereas all other properties of the nonequilibrium flow [Eqs. (11–13)] were calculated with finite difference solvers on the grid nods. The corresponding coupling values were determined by interpolation. As boundary conditions at the outer edge of the jet and the outflow cross section the pressure is set to a constant value of 2.9 mbar. All other values are extrapolated normally to the boundary. At the symmetry axis all values are reflected, except the electron and vibrational temperature, which are extrapolated to the symmetry axis as a boundary line of the finite difference grid.

Figure 8 shows the heavy particle temperature and Fig. 9 shows the electron temperature at the two cross sections, respectively. The numerical results for the first cross section (x = 50 mm) are the interpolation of the cell center values of a finite volume calculation, and so these values represent already an average value of the first cell close behind the inflow cross section. The calculated electron temperature at the 300 mm cross section shows good agreement with the measured values in the center of the jet, while a higher discrepancy is noted with increasing radial distance. The heavy particle temperature shows generally a higher difference. However, this temperature was only measured at the position in the center of the jet (y = 0 mm), and the distribution is calculated with the obtained ratio to the electron temperature. The calculated value at y = 0 mm is within the error bar given by the electrostatic crossed probe measurements (T = 5150 K ± 2200 K). In the center of the jet the vibrational temperature is calculated to be close to the electron temperature. Thus, the estimation made in Sec. III ($T_{vib} = T_e$) is partially valid as shown by these results, especially at positions of interest for material tests. With increasing distance from the center, the vibrational temperature tends more to the heavy particle temperature.

Figure 10 depicts the velocity distributions at the two cross sections, Fig. 11 shows the axial development, and Fig. 12 the calculated velocity distribution as vector map. The agreement with the measured values is quite good, although the calculated velocity is slightly underpredicted behind the inflow cross section, whereas it is overpredicted downstream. This could be most likely explained by too high viscosity for the high-temperature parameter range and by too low effective viscosity further downstream because of the turbulent entrainment that was not taken into consideration yet. Figure 12 clarifies that the effective flow diameter is increasing downstream as shown also by the measurements.

Additionally, to the given number densities for N, N_2, and e (Sec. III), a small amount of ionized molecules is taken into account, thus, allowing the use of the complete chemical equation set. Of course, electrical quasineutrality is respected.

Figure 13 shows the number densities at the two investigated cross sections, and Fig. 14 shows the axial distribution. Generally, the agreement is qualitatively and quantitatively good. The calculated total number density at a distance of 300 mm is slightly lower than the measured one. This is caused by the higher temperature encountered in the calculation as shown already in Fig. 8. The latter influences also the electron number density that is higher in the calculation. Figures 13

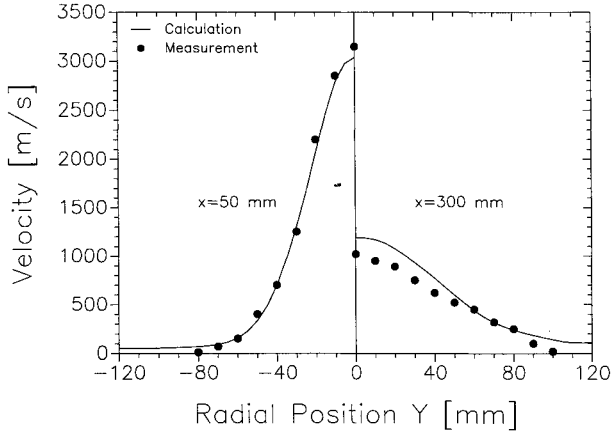

Fig. 10 Velocity at the two cross sections.

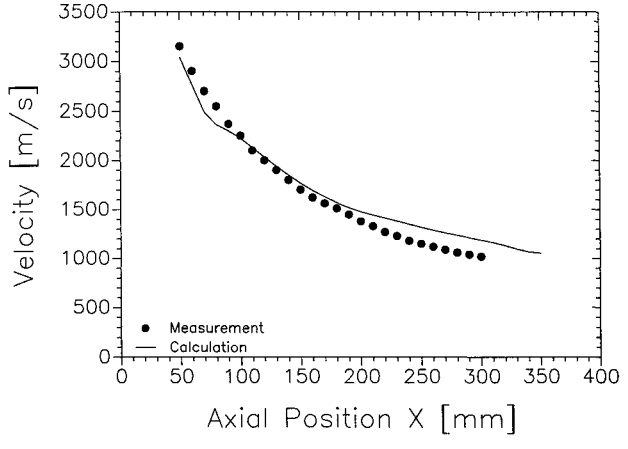

Fig. 11 Velocity vs axial position in the center of the plasma plume.

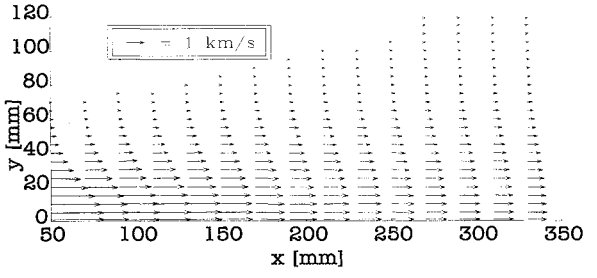

Fig. 12 Calculated vector velocity distribution.

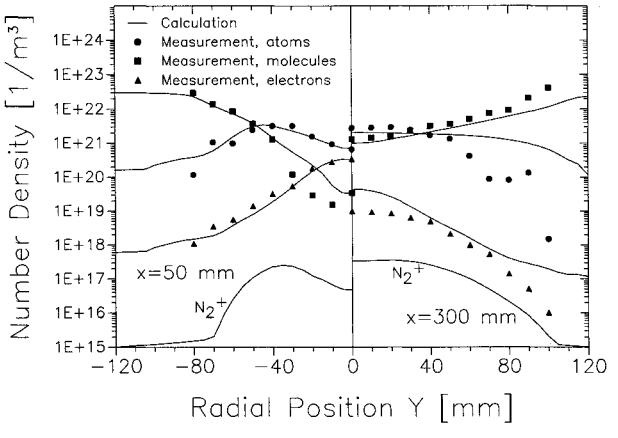

Fig. 13 Number densities at the two cross sections.

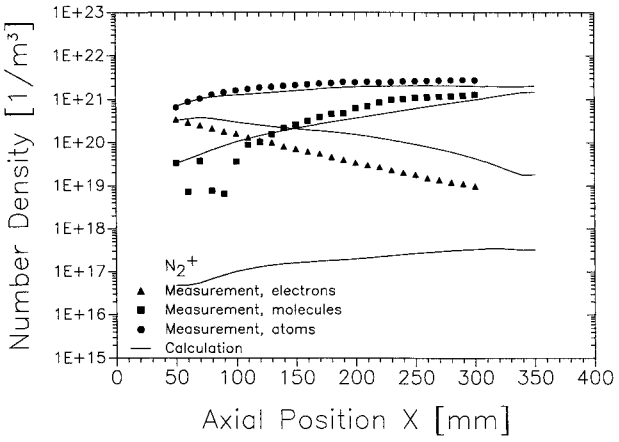

Fig. 14 Number densities vs axial position in the center of the plasma jet.

and 14 clarify also the limits of the method used to determine the local number densities from the performed measurements. If the mole fraction of atomic or molecular nitrogen is low (<3–4%) their portion to the total energy of the flow is low, too. Therefore, the determination of the corresponding number density is very sensitive and not accurate, as may be seen from the results for the molecular number density at small distances to the plasma source.

The total mass flux ratio of the outflow to the inflow cross section is calculated to about 1.8, for comparison, the measurements give a higher value of 2.4. This difference could be caused by the turbulent character of the flow that was neglected in the numerical simulation. However, the local Reynolds number on the symmetry axis at the 50 mm position is only about 100 (related to the local jet diameter), increasing with the axial position to about 250 at the 300 mm cross section. Therefore, the contribution of the turbulence to the total viscosity is small. Other influences are given by small inaccuracies in the determination of the velocity, especially for the radial component that was not available from the measurements and by the calculation of the viscosity with the Yos model.[34] Therefore, verification with other viscosity and turbulence models is desirable.

VII. Summary and Conclusions

A nitrogen high-enthalpy plasma flow within a plasma wind tunnel, which is neither in thermal nor in chemical equilibrium, was the subject of an experimental and numerical investigation at the Institut für Raumfahrtsysteme of the University of Stuttgart. Measurements along the plasma axis were performed to determine the stagnation pressure, heat flux, velocity, electron density, and temperature of the flowfield. Two cross sections were selected for measurements of radial distributions. With the obtained data it was possible to calculate the local specific enthalpies, mass fluxes, and number densities of molecular, atomic, and ionized nitrogen. A comparison of the mole fractions obtained with this method with mass spectrometry measurements showed a very good agreement.

The integration of the local mass flux distributions shows that the flow is entraining and accelerating the ambient gas, and thus lowering the specific energy. The total mass flux at the second cross section is about 2.4 times the flux through the plasma source, and, corresponding to this, the mean specific enthalpy is only about 40% of the value at the plasma source exit. This turbulent entrainment of ambient gas will be the subject of further experimental and numerical investigations.

Measurements with different catalytic probes clearly showed the influence of the surface material and surface temperature on the heat flux transferred to the body. For example, at a distance of $x = 300$ mm to the plasma source, the heat flux on a SiC probe is only about half the heat flux to a copper body.

The determination of the species number densities, the temperatures, and velocities gave the possibility to validate the numerical method used at the IRS for the calculation of nonequilibrium high-enthalpy flows. Taking the experimental results at $x = 50$ mm as initial and inflow boundary conditions, the flowfield was calculated with a Navier–Stokes code. This code was developed and tested in order to gain a more profound understanding of the fundamental processes occurring in high-enthalpy flows like plasma wind tunnels or hypersonic expansion nozzles. The code system was implemented for airflow. For the present investigation the code system was reduced to a pure nitrogen flow, including nonequilibrium chemistry and vibrational and electron energy equations. The nonequilibrium chemistry model includes also the ionized nitrogen species. The electron temperature has a strong effect on the transport properties in the ionized region. Therefore, models for the transport properties of nitrogen and air were developed and investigated. With respect to the physical complexity of the problem the agreement of the measured and calculated results is good.

Therefore, with this test program it is shown that the IRS plasma wind-tunnel conditions can be evaluated in a manner that they can be used for the validation of nonequilibrium high-enthalpy codes.

Further investigation of these test conditions is planned with nonintrusive measurement techniques, i.e., emission spectroscopy and Fabry–Perot interferometry. Additionally, the numerical calculation of the plasma source to obtain and compare the local mass fluxes at the first cross section and the consideration of a turbulence model are in preparation.

The extension to an air plasma flow will then be the next experimental and computational iteration step of this research program.

Acknowledgments

This work was supported in part by the Sonderforschungsbereich SFB 259, "Hochtemperaturprobleme rückkehrfähiger Raumtransportsysteme" of the Deutsche Forschungsgemeinschaft and by the Aviation Marcel Dassault, Grant H-ST-1-1135-AMD. The authors wish to thank all other coworkers of the PWK simulation group at the IRS for their assistance in performing the experiments and T. Gogel for the evaluation of the radiation losses.

References

[1]Lukasiewicz, J., Whitfield, J. D., and Jackson, R., "Aerodynamic Testing at Mach Numbers from 15 to 20," *Proceedings of the ARS International Hypersonic Conference* (Cambridge, MA), 1961.

[2]Hornung, H., "High Enthalpy Wind Tunnel for the Simulation of Chemical Non-Equilibrium Effects," DLR, Institut für Experimentelle Strömungsmechanik, Doc. IB222-86A43m, 1986.

[3]Auweter-Kurtz, M., "Lichtbogenantriebe für Weltraumaufgaben," B. G. Teubner, Stuttgart, Germany, 1992.

[4]Wilhelmi, H., private communication,"Der Hochenthalpie-Windkanal des Instituts für Industrieofenbau RWTH Aachen," Aachen, Germany, 1990.

[5]Charpentier, P., and Leroux, R., "SIMOUN—Un Nouveau Moyen d'Essais Pour le Developpement des Protections Thermiques d'HERMES," *Proceedings of the ESA Symposium on Space Applications of Advanced Structural Materials*, ESA SP-303, ESTEC, Noordwijk, 1990.

[6]Kindler, K., private communication, "The Arc Heated Wind Tunnel of DLR—A Tool for Material Research," DLR, Cologne, Germany, 1989.

[7]Russo, G., "Scirocco Hermes Thermal Protection Qualification Facility," *Proceedings of the 2nd HERMES Industry Day*, Munich, Germany, 1990.

[8]Rochelle, W. C., Battley, H. H., Grimaud, J. E., Tillian, D. J., Murray, L. P., Lueke, W. J., and Heaton, T. M., "Orbiter TPS Development and Certification Testing at the NASA/JSC 10MW At-

mospheric Reentry Materials and Structure Evaluation Facility," AIAA Paper 83-0147, Jan. 1983.

[9]Arepalli, S., Yuen, E. H., and Scott, C. D., "Application of Laser Induced Fluorescence for Flow Diagnostics in Arc Jets," AIAA Paper 90-1763, June 1990.

[10]Laure, S., Auweter-Kurtz, M., Fasoulas, S., Habiger, H. A., and Röck, W., "The IRS Plasma Wind Tunnels as a Tool for the Investigation of Planet Entry Missions," AIAA Paper 92-3886, July 1992.

[11]Scott, C. D., "Survey of Measurements of Flow Properties in Arc Jets," *Journal of Thermophysics and Heat Transfer*, Vol. 7, No. 1, 1993, pp. 9–24.

[12]Fasoulas, S., Auweter-Kurtz, M., and Habiger, H. A., "Experimental Investigation of a Nitrogen High-Enthalpy Flow," *Journal of Thermophysics and Heat Transfer*, Vol. 8, No. 1, 1994, pp. 48–58.

[13]Schönemann, A., and Auweter-Kurtz, M., "Characterization of Nitrogen and Air Plasma Flows by Mass Spectrometry," ISPC11, 11th International Symposium of Plasma Chemistry, Loughborough, 1993.

[14]Schönemann, A., Auweter-Kurtz, M., Habiger, H. A., Sleziona, P. C., and Stöckle, T., "Analysis of the Argon Additive Influence on a Nitrogen Arcjet Flow," *Journal of Thermophysics and Heat Transfer*, Vol. 8, No. 3, 1994, pp. 466–472.

[15]Sleziona, P. C., Auweter-Kurtz, M., and Schrade, H. O., "Computation of MPD Flows and Comparison with Experimental Results," *International Journal for Numerical Methods in Engineering*, Vol. 34, Wiley, New York, 1992.

[16]Sleziona, P. C., Auweter-Kurtz, M., Glocker, B., Gogel, T., Gölz, T., Messerschmid, E., and Schrade, H. O., "Non-Equilibrium Flow in Arc Heated Wind Tunnel," *Hypersonic Flows for Reentry Problems*, edited by J.-A. Desideri, R. Glowinski, and J. Periaux, Vol. 2, Springer–Verlag, Berlin, 1991.

[17]Eberle, A., "Characteristic Flux Averaging Approach to the Solution of Euler's Equations," VKI Lecture Series, Computational Fluid Dynamics, 1987-04, 1987.

[18]Schmatz, M. A., Brenneis, A., and Eberle, A., "Verification of an Implicit Relaxation Method for Steady and Unsteady Viscous and Inviscid Flow Problems," AGARD Symposium on Validation of Computational Fluid Dynamics, AGARD CP437, Vol. 1, Lisboa, Portugal, 1988.

[19]Park, C., "Convergence of Computation of Chemically Reacting Flows," *Thermophysical Aspects of Re-Entry Flows*, Vol. 103, Progress in Astronautics and Aeronautics, AIAA, New York, 1986, pp. 478–513.

[20]Park, C., "Nonequilibrium Hypersonic Aerothermodynamics," Wiley-Interscience, New York, 1990.

[21]Park, C., Howe, J. T., Jaffe, R. L., and Candler, G. V., "Chemical-Kinetic Problems of Future NASA Missions," AIAA Paper 91-0464, 1991.

[22]Elsner, M., "Thermal Protection System Comparison of the HERMES Flight Environment and Test Facility Environment of the IRS Plasma Wind Tunnel," MBB-Rept. H-NT-1B-0006-MBB, Oct. 1990.

[23]Pope, R. B., "Stagnation Point Convective Heat Transfer in Frozen Boundary Layers," *AIAA Journal*, Vol. 6, No. 4, 1968, pp. 619–626.

[24]Marvin, J. G., and Pope, R. B., "Laminar Convective Heating and Ablation in the Mars Atmosphere," *AIAA Journal*, Vol. 5, No. 2, 1967, pp. 240–248.

[25]Pope, R. B., "Measurements of Enthalpy in Low Density Arc Heated Flows," *AIAA Journal*, Vol. 6, No. 1, 1968, pp. 103–110.

[26]Vojvodich, N. S., and Pope, R. B., "The Influence of Ablation on Stagnation Region Convective Heating for Dissociated and Partially Ionized Boundary Layer Flows," *Proceedings of the 1965 Heat Transfer and Fluid Mechanics Institute*, Stanford Univ. Press, Stanford, CA, 1965, pp. 114–137.

[27]Boison, J. C., and Curtiss, H. A., "An Experimental Investigation of Blunt Body Stagnation Point Velocity Gradient," *ARS Journal*, Vol. 29, No. 2, 1959, pp. 130–135.

[28]Goulard, R., "On Catalytic Recombination Rates in Hypersonic Stagnation Heat Transfer," *Jet Propulsion*, Vol. 28, No. 11, 1958, pp. 733–745.

[29]Fay, J. A., and Riddell, F. R., "Theory of Stagnation Point Heat Transfer in Dissociated Air," *Journal of the Aeronautical Sciences*, Vol. 25, No. 2, 1958, pp. 73–85.

[30]Rosner, D. E., "Similitude Treatment of Hypersonic Stagnation Point Heat Transfer," *ARS Journal*, Vol. 29, No. 3, 1959, pp. 215, 216.

[31]Fruchtmann, I., "Temperature Measurements of Hot Gas Streams," *AIAA Journal*, Vol. 1, No. 8, 1963, pp. 1909, 1910.

[32]Hartunian, R. A., Thompson, W. P., and Safron, S., "Measurements of Catalytic Efficiency of Silver for Oxygen Atoms and the O-O_2 Diffusion Coefficient," *Journal of Chemical Physics*, Vol. 43, 1965, pp. 4003–4006.

[33]Anderson, L. A., "Effect of Surface Catalytic Activity on Stagnation Heat-Transfer Rates," *AIAA Journal*, Vol. 11, No. 5, 1973, pp. 649–656.

[34]Yos, J. M., "Transport Properties of Nitrogen, Hydrogen, Oxygen and Air To 30,000°K," TM RAD-TM-63-7, Avco Corp., 1963.

[35]Okuno, A. F., and Park, C., "Stagnation-Point Heat-Transfer Rate in Nitrogen Plasma Flows: Theory and Experiment," *Transactions of the ASKE*, Aug. 1970; also *Journal of Heat Transfer*, Aug. 1970, pp. 372–384.